RSC Advances

PAPER

View Article Online
View Journal | View Issue

Cite this: *RSC Adv.*, 2023, **13**, 26445

Near-infrared active ferrocenyl porous organic polymer with photothermal enhanced enzymatic activity for combination antibacterial application†

Lei Wang, [a] Lin Shi,[a] Taoyan Guo,[b] Jingsong Yuan,[b] Baolong Zhou [*b] and Jing Zhang*[a]

As a severe ongoing global problem, bacterial contamination exists in every aspect of human life and the search for new antibacterial agents is urgently needed. Herein, a ferrocenyl porous organic polymer (FMC-POP) broad-spectrum antibacterial agent based on synergistic photothermal and peroxidase-like activity was prepared in a facile manner *via* the copolymerization of ferrocene diformaldehyde and cinnamaldehyde with mannitol through the acid-responsive acetal bond. The photoactive FMC-POP, with high photothermal conversion efficiency (41.45%), could convert not only the near-infrared laser irradiation into local heat to eradicate bacteria, but also low-concentration H_2O_2 into radical oxygen species (˙OH) that are effective against bacteria. Compared with single-mode photothermal (PTT) and enzymatic therapies, this combination therapy could significantly improve the bactericidal effect, exhibiting a germicidal efficiency of up to 99% (*vs.* 80.42% for PTT and 70% for enzyme). Thus, our work paves the way for a synergistic non-invasive antimicrobial therapy, which could expand the applications of POP-based artificial enzymes in biomedicine.

Received 3rd June 2023
Accepted 23rd August 2023

DOI: 10.1039/d3ra03504b

rsc.li/rsc-advances

Introduction

Bacterial infections, especially those concerned with antibiotic-resistant bacteria that are mainly ascribed to the abuse of antibiotics, have emerged as one of the most challenging issues to threaten human health.[1–3] The dissemination of antibiotic-resistant genes has become almost inevitable, and has already become prevalent in many common pathogenic strains. Therefore, urgent action is required to develop novel antibacterial agents as alternatives to synthetic antibiotics, to address this growing crisis.[4,5]

Antibiotic-free strategies, that is, exerting bactericidal action without using antibiotics, has emerged as a promising approach to respond to the current dilemma in bacterial infection.[6] Hitherto, several types of antibiotic-free strategies with concurrently high efficacy and lower side effects have been developed to fight against multidrug-resistant bacteria, such as photothermal therapy (PTT), ultrasound therapy, as well as enzyme therapy.[7–9] Among these strategies, PTT, as a non-invasive approach, works through photothermal conversion to evoke bacteria death.[10,11] Enzyme therapy exerts antibacterial activity through the generation of reactive oxygen species (ROS), to induce irreversible oxidative damage to bacteria.[12,13]

Hydrogen peroxide (H_2O_2) is a typical ROS, which has been frequently applied in clinical practice.[14] In order to achieve germicidal efficacy, relatively high concentrations are commonly required, which also causes damage to normal tissues.[15] Thus, it is urgently desired to enhance the antibacterial performance of H_2O_2 at lower concentrations. As the most well-known organometallic compound, ferrocene, as well as its derivatives, have attracted significant research interest, and have been extensively studied in the biomedical field, either directly as drugs or as precursors to find new drugs with reasonable enhancements.[16–18] One of the most prominent features of ferrocene is its intrinsic enzymatic activity to perform peroxidase-like catalytic therapy, converting H_2O_2 into toxic hydroxyl radical, which has been widely used in the biomedical field.[19] However, frequent reports have confirmed that this single-mode therapy is still hampered by its limited antibacterial activity. To enhance the therapeutic effect, combinational therapy, such as the use of joint PTT and enzyme therapy, has gained increasing attention. Such an approach can not only finely tune the treatment effect of the respective single-mode therapy, but also achieve synergistic amplification of the therapeutic effects.[20] The key problem is how to integrate different therapies into a single platform.[21]

Porous organic polymers (POPs) are an emerging class of lightweight and multifunctional network materials built from

[a]*The First Affiliated Hospital of Weifang Medical University (Weifang People's Hospital), Weifang Medical University, Weifang, 261031, Shandong, PR China. E-mail: zhangjing_wy@126.com*

[b]*School of Pharmacy, Weifang Medical University, Weifang, 261053, Shandong, PR China. E-mail: zhoubaolong@wfmc.edu.cn*

† Electronic supplementary information (ESI) available. See DOI: https://doi.org/10.1039/d3ra03504b

covalently linked organic structural units.[22] The pure organic structure endows POPs with unique physicochemical properties, such as good biocompatibility, large specific surface area, high porosity and excellent stability, as well as customizable structure and functionality, which is used in a variety of applications, ranging from environmental to biomedical, gas storage and separation, heterogeneous catalysis, biomedicine, sensing, optoelectronics and energy storage and conversion.[23–27] The localized structural environment provides a precise and accessible void space, which increases reactant exposure on the catalyst surface and thus improves the catalytic efficiency.[28,29] Based on the above characteristics, multiple functional ferrocene-based porous organic polymers with immobilized metal sites can be constructed, conferring peroxidase activity to realize combined therapy.

Here, a ferrocene-based porous organic polymer with excellent enzyme-mimicking activity, denoted as FMC-POP and which could work as a therapeutic platform exerting combination treatment, was developed as a broad-spectrum antibacterial agent. On one hand, FMC-POP combines the inherent features of the porous organic polymer and ferrocene and can retain the characteristics of ferrocene to convert low-concentration H_2O_2 into $^{\bullet}OH$ to resist bacteria, thus exerting enzymatic treatment. On the other hand, FMC-POP also presents prominent photothermal activity to convert near-infrared (NIR) laser irradiations into hyperthermia, thus further enhancing the enzymatic activity against bacteria. The antibacterial performance of H_2O_2 utilizing the peroxidase-like activity of FMC-POP against both Gram-negative bacteria (*Escherichia coli*) and Gram-positive bacteria (*Staphylococcus aureus*) was greatly improved under the NIR laser. Therefore, this work offers a new synergistic antibacterial strategy, which further expands the application of POP-based artificial enzymes in biomedicine.

Results and discussion

As can be seen in Scheme 1, FMC-POP connected through the acid-responsive acetal bond was quantitatively prepared using a ternary copolymerization strategy between the medicinal monomers, in which the monomer containing aldehyde groups (ferrocene diformaldehyde and cinnamaldehyde) reacted with the building block bearing polyhydroxy groups, *i.e.*, mannitol, under catalysis with *p*-toluenesulfonic acid in the solvent *o*-dichlorobenzene.[30] The details are given in the ESI.† FMC-POP was obtained as a black-brown powder, which was insoluble in conventional organic solvents (Fig. S2†). However, owing to the introduction of an O-rich acetal bond linkage, FMC-POP dispersed well in water.

Construction of the target polymer was verified by Fourier-transform infrared (FT-IR) spectroscopy. As shown in Fig. 1a, the FT-IR of FMC-POP combined the features of all the building blocks, for which the vibrations ascribed to cinnamaldehyde (styryl at 1440 cm^{-1}),[31] ferrocene (1601 cm^{-1}),[32] as well as the vibration of mannitol (saturated carbon at 2901 cm^{-1})[33] could be clearly observed. Meanwhile, the disappearance of the aldehyde group in the FT-IR of FMC-POP, together with the appearance of the characteristic vibration belonging to the acetal ring (1704 cm^{-1}), demonstrated formation of the polymer skeleton.[34] Similar to other reports, the powder X-ray diffraction (XRD) of FMC-POP shown in Fig. 1b displayed only a broad peak around 25°, which revealed the amorphous structure of the as-synthesized polymers.[35]

To investigate the porosity of the as-synthesized FMC-POP, the low-temperature N_2 absorption–desorption curve was determined. It can be seen clearly that FMC-POP displayed an isotherm combining the features of type I and type IV isotherms simultaneously (Fig. 1c).[36] As can be seen, a near vertical uptake was found at the low pressure range ($P/P_0 < 0.05$), implying the existence of micropores.[37] Meanwhile, the large hysteresis loop at the branch of the absorption and desorption curve, together with the quick uptake in the high pressure range ($0.5 < P/P_0 < 1.0$), revealed the concurrent existence of mesopores and macropores, which are beneficial for thermal conduction.[38,39] The hierarchical pore structure can also be directly observed from the pore-size distribution curve analyzed using the density functional theory method (Fig. 1d), with the pore-size distribution ranging from 1.8 nm to 25 nm. This distribution of pore sizes ranges from mesoporous to microporous, with the main peak centered at 1.41 nm. The Brunauer–Emmett–Teller surface area of FMC-POP was calculated as 274.42 $m^2\ g^{-1}$, with an accumulative pore volume (V_{total}) of 0.594 $m^3\ g^{-1}$. The thermal stability, as an important parameter for phototherapeutic agents, was measured using thermogravimetric analysis. It should be noted that FMC-POP is stable up to 180 °C, with only a certain amount of weight decrease that can be attributed to volatilization of solvent strongly adsorbed onto the material. Subsequently, slow and continuous weight reduction originating from decomposition of the FMC-POP was found. At 800 °C, the final residual weight was higher than 50% (Fig. S3†), indicating the good thermal stability of FMC-POP.

Scanning electron microscopy (SEM; Fig. 2a–c) and transmission electron microscopy (TEM; Fig. 2d and e) were conducted to illustrate the micromorphology of the as-synthesized FMC-POP.[40] One can clearly see that FMC-POP is composed of a stalactite-shaped morphology constructed from interconnected, nearly spherical particles with honeycomb-like pores at the nanometer to micrometer scale. Meanwhile, the hierarchical porous structure (with concurrent micropores, mesopores and macropores) can be clearly observed from the SEM and TEM images, as well as the light and shade contrast from the high-resolution TEM (HR-TEM; Fig. 2f). Meanwhile, there are no crystal streaks in the HR-TEM images, further indicating the amorphous structure of the as-synthesized polymers.[41] The elemental mapping (Fig. 2g) and corresponding energy dispersive spectrometry (Fig. S4†) revealed the homogeneous distribution of O (12.47 at%), C (83.41 at%) and Fe (3.86 at%) on the porous matrix.

To effectively combat bacterial-related infections, photothermal agents must feature excellent light stability as well as effective recycling stability, and these features need to be evaluated.[42] Before exploring the photothermal effect of FMC-POP, the UV-vis-NIR absorption spectrum was first examined at a concentration of 150 μg mL^{-1}. As seen from Fig. S5,† FMC-

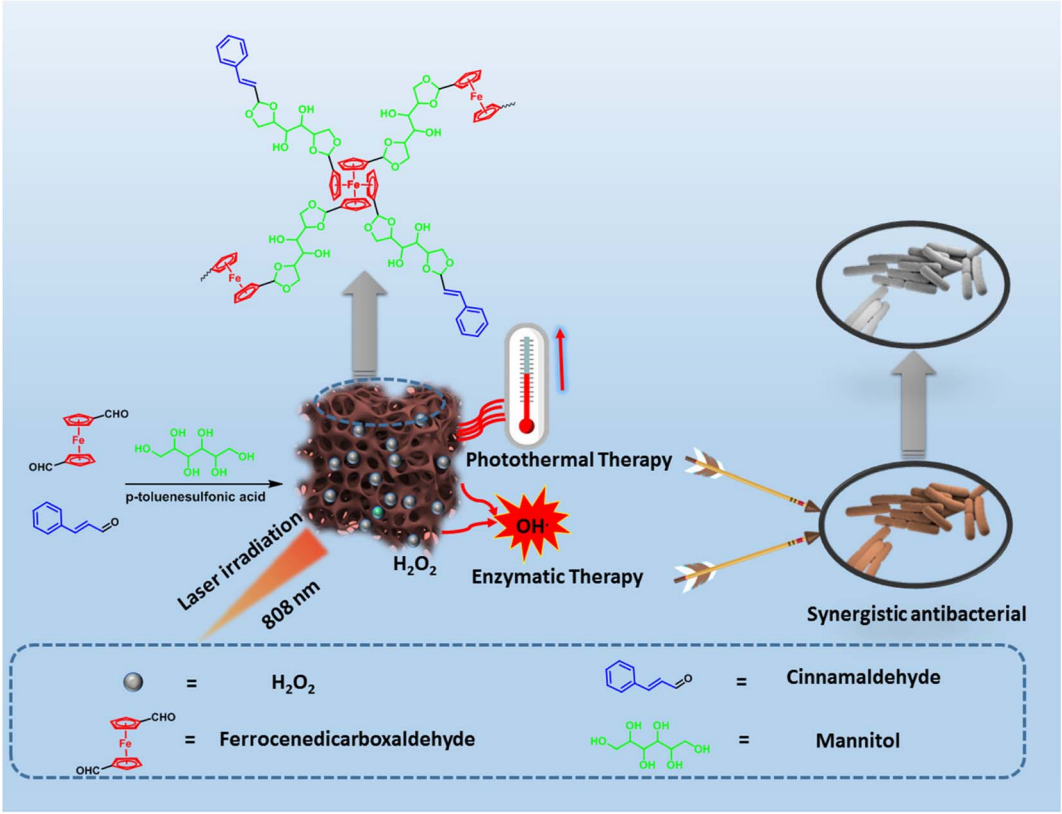

Scheme 1 Route for the synthesis of FMC-POP *via* the ternary copolymerization strategy and the schematic of the synergistic antibacterial mechanism.

POP presented a strong absorption in the wavelength range from 400 to 1000 nm, still maintaining a certain intensity in the biologically friendly and tissue-permeable NIR region.[43] This result demonstrated that the as-synthesized FMC-POP had an excellent light-thermal response, endowing it with great application potential as a PTT agent in the NIR range.[44] Fig. 3a shows the concentration-dependent temperature change behavior of FMC-POP under NIR irradiation (808 nm) for 10 min. As can be seen, the temperature of the FMC-POP aqueous solution increased with increasing concentration, and a maximum temperature of 55.6 °C can be reached with 150 μg mL^{-1} after 10 min of irradiation, which is much higher than for pure water (30.1 °C). The temperature could increase to 47.4, 50.1 and 51.9 °C at low FMC-POP concentrations of 50, 75 and 100 μg mL^{-1}, respectively. Similar results were also found from the heating photographs of the FMC-POP suspension captured *via* an infrared thermal camera (Fig. 3c), whereby the temperature had risen with increase in FMC-POP concentration. Fig. 3d shows the reversibility of the photothermal capacity for FMC-POP. It can be seen clearly that FMC-POP still retained a similar efficiency after NIR laser irradiation for five consecutive on/off cycles. Such a result verifies that FMC-POP could be used repeatedly in real applications.[45] Fig. 3e demonstrates the heating and cooling profile of FMC-POP (150 μg mL^{-1}) upon 808 nm laser irradiation for a single on/off cycle, from which a linear relationship between time and $-\ln\theta$ was obtained based on the cooling process (Fig. S6†). The photothermal conversion efficiency of FMC-POP was obtained with reference to the photothermal conversion equations (eqn (S1)–(S3)†) and was calculated as 41.45%. The high photothermal conversion efficiency of FMC-POP could not only be favorable for the utilization of light energy for conversion into local heat to boost sterilization, but also be effective in reducing the sample consumption.[46] Additionally, the photostability of FMC-POP was confirmed by small changes in its UV absorbance (Fig. S7†) after irradiation with a laser (1.0 W cm^{-2}) at different time intervals (0 min, 1 min, 3 min, 5 min and 7 min). All these results demonstrate the great potential for application of FMC-POP as an effective NIR thermal agent.

The enzymatic activity of FMC-POP to catalyze decomposition of hydrogen peroxide (H_2O_2) to produce the highly lethal hydroxyl radicals ($^{\bullet}OH$) was assayed using 3, 3′, 5, 5′-tetramethylbenzidine (TMB) and H_2O_2 as dual substrates, where TMB, as an indicator, could be oxidized by $^{\bullet}OH$, causing a visible color change and the emergence of an absorption at 652 nm.[47] The possible catalytic mechanism is illustrated in the ESI,† and is mainly attributed to the conversion of hydrogen peroxide (H_2O_2) by ferrous (Fe^{2+}) ions in the ferrocene units to generate hydroxyl radicals ($HO^{\bullet}$). As presented in Fig. 4a, only in the solution containing the dual substrates and FMC-POP simultaneously does the clear blue and intense absorption peak at 652 nm appear. In line with previous reports, FMC-POP

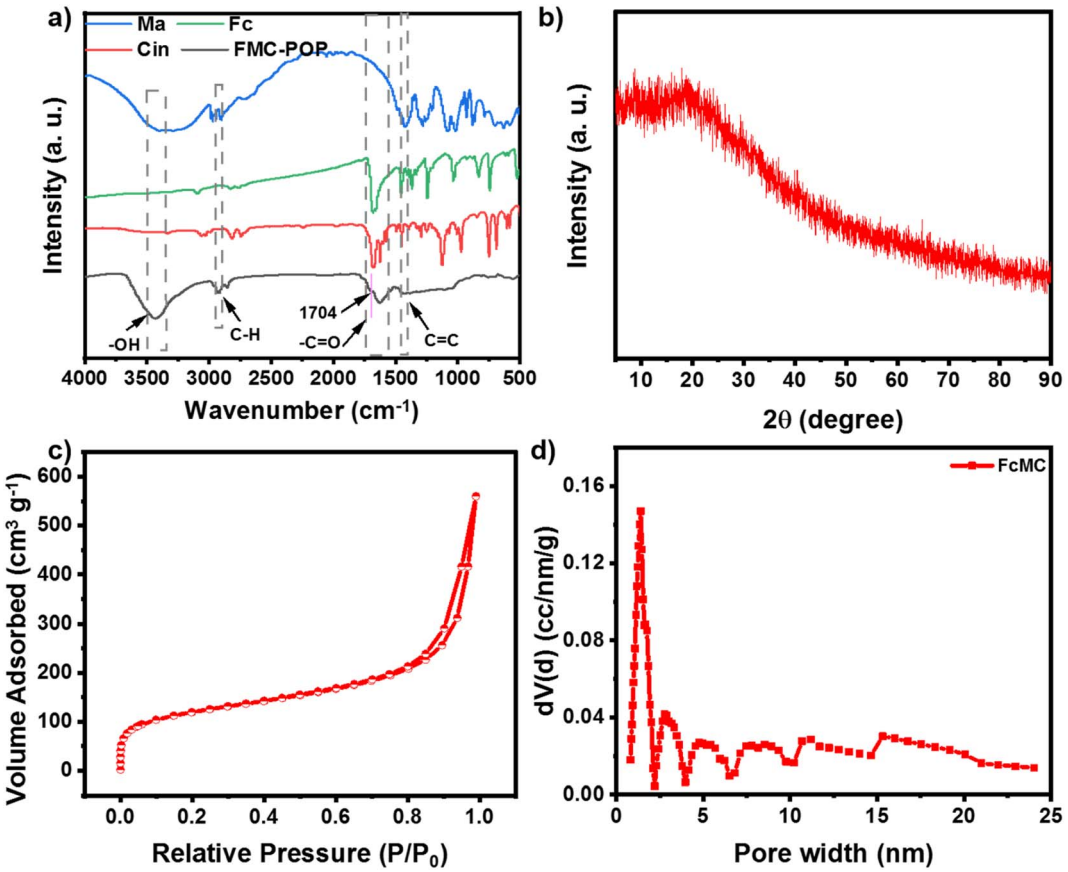

Fig. 1 Physical characterization of FMC-POP. (a) FT-IR of FMC-POP, as well as of the reaction monomers used for the synthesis of FMC-POP. (b) Powder XRD of FMC-POP. (c) Low-temperature N_2 uptake isotherm. (d) Pore-size distribution curve of FMC-POP.

displayed a concentration-dependent enzyme catalysis activity, which was positively correlated with the concentration of FMC-POP, as revealed by the enhanced UV absorption at 652 nm (Fig. 4b). Furthermore, similar to previous reports, at a fixed H_2O_2 concentration (10 mM), the pH value plays a decisive role in the enzymatic activity, which initially increased with decrease in pH, but then decreased. The maximum activity appeared at a pH of 3.5 (Fig. 4c). Under weak acidic conditions (pH = 5.5 and 6.5), FMC-POP still presented visible peroxidase-like activity, providing the foundation for real application in the treatment of bacterial infections. It is worth noting that the absorption intensity of TMB under irradiation with the NIR laser was substantially higher than under laser-free conditions, indicating that the NIR laser played a crucial role in enhancing the peroxide-like enzymatic activity of FMC-POP (Fig. 4d).[48] The temperature increase ascribed to the photothermal activity excited by the laser irradiation further promoted the enzyme-like activity of FMC-POP, which is strongly connected to the temperature. Furthermore, the generation of $^{\bullet}OH$ could also be validated by electron paramagnetic resonance (EPR) spectroscopy. As displayed in Fig. S8,† a typical EPR four-peak spectrum of DMPO-OH was detected, indicating that $^{\bullet}OH$ was produced when FMC-POP was exposed to H_2O_2.

The above experiments demonstrate the effectiveness of the dual-mode synergistic photothermal and enzymatic bactericidal activity, which could enhance the production of $^{\bullet}OH$ from H_2O_2 under weak acid conditions. Based on this, we concluded that FMC-POP could be used as a promising therapeutic agent realizing joint enzymatic and photothermal therapy for bacterial infections. Therefore, the synergetic antibacterial effect of FMC-POP *in vitro* was evaluated *via* the plate counting method.[49] For comparison, samples were divided into seven treatment groups, including (I) phosphate buffered saline (PBS), (II) FMC-POP, (III) H_2O_2, (IV) laser, (V) FMC-POP + H_2O_2, (VI) FMC-POP + laser and (VII) FMC-POP + H_2O_2 +laser, to thoroughly evaluate the antibacterial performance against both *S. aureus* and *E. coli*. During the experiment, PBS with pH = 5.5 was used to simulate the microenvironment of bacterial infection.[50] As presented in Fig. 5a, similarly to the PBS group (I), a large number of viable colonies were observed from the LB agar plates in groups (II) (FMC-POP) and (IV) (laser), indicating that NIR irradiation and FMC-POP alone could not affect the bacterial growth (laser group: the survival rate was 97% and 99% for *E. coli* and *S. aureus*, respectively; FMC-POP group: *E. coli* survival 80%, *S. aureus* survival 90.9%). Meanwhile, only a weak antibacterial effect was observed for group (III) (H_2O_2) (*E. coli* survival 78%, *S. aureus* survival 78.78%), which could be assigned to the poor bactericidal efficacy of H_2O_2 towards *S. aureus* and *E. coli* at low concentrations of hydrogen peroxide (10 mM). By contrast, the number of colonies when treated with (V) (FMC-POP + H_2O_2)

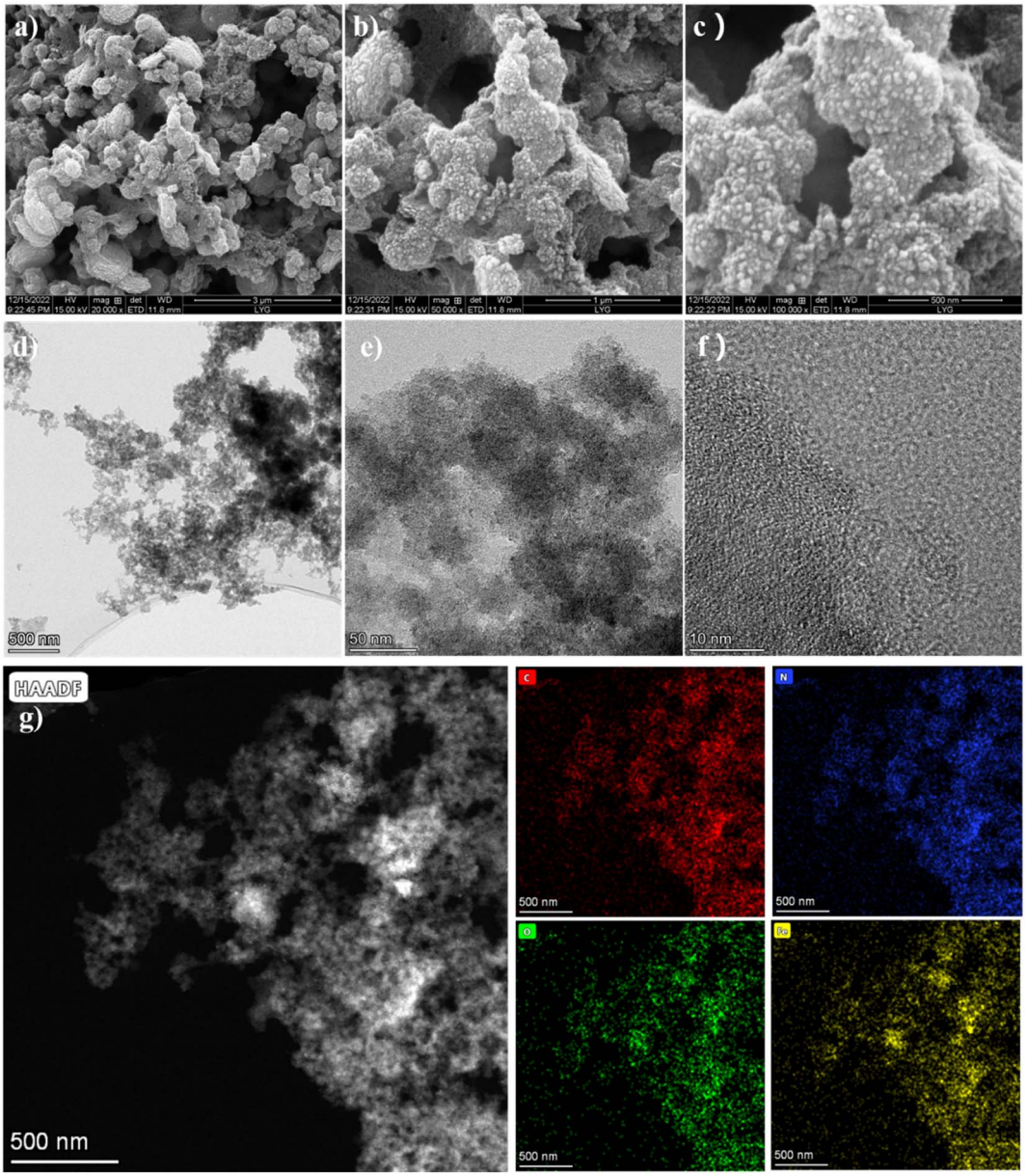

Fig. 2 SEM and TEM images of FMC-POP. (a–c) SEM of FMC-POP, scale bars of 3 μm, 1 μm and 500 nm, respectively. (d and e) TEM of FMC-POP, scale bars of 500 and 50 nm, respectively. (f) HR-TEM of FMC-POP, with scale bar of 10 nm. (g) Elemental mapping of FMC-POP.

was greatly reduced, decreasing to 30.62% and 26.67% survival for *S. aureus* and *E. coli*, respectively. This result verified that FMC-POP could catalyze the decomposition of H_2O_2 into toxic $^{\bullet}OH$, leading to bacterial death. All these results demonstrate that treatment relying on single-mode PTT and enzymatic therapy material alone cannot achieve an ideal sterilization effect. Compared with groups (II) (FMC-POP), (III) (H_2O_2), (IV) (laser) and (V) (FMC-POP + H_2O_2), as well as group (VI) (FMC-POP + laser), bacteria incubated with group (VII) (FMC-POP + H_2O_2 + laser; 808 nm laser, at 1.2 W for 10 min) presented a significantly reduced survival rate, with the germicidal efficiency reaching 99.1% for both *E. coli* and *S. aureus* with only a few colonies. This result confirmed the successful construction of the enzyme/PTT synergetic antibacterial system. Subsequently, a live–dead bacterial cell staining assay was conducted to show more intuitively the response *in vitro* for the antibacterial effect.[51] Viable bacteria with an intact cell membrane were stained with green fluorescence using calcein-AM.[52] By contrast, dead bacteria with damaged cell membranes were stained with red fluorescence using propidium iodide.[53] As presented in Fig. 5c and e, for bacteria treated with PBS and FMC-POP, as well as the laser treatment group, only an intense green fluorescence could be detected, whereas a weak red fluorescence was observed for bacteria treated with H_2O_2, FMC-POP + H_2O_2 and FMC-POP + laser. It is worth noting that all the bacteria showed red fluorescence when treated with FMC-POP + H_2O_2 + laser. As can be seen from Fig. 5d and f, *E. coli* and *S. aureus* displayed similar responses towards the different

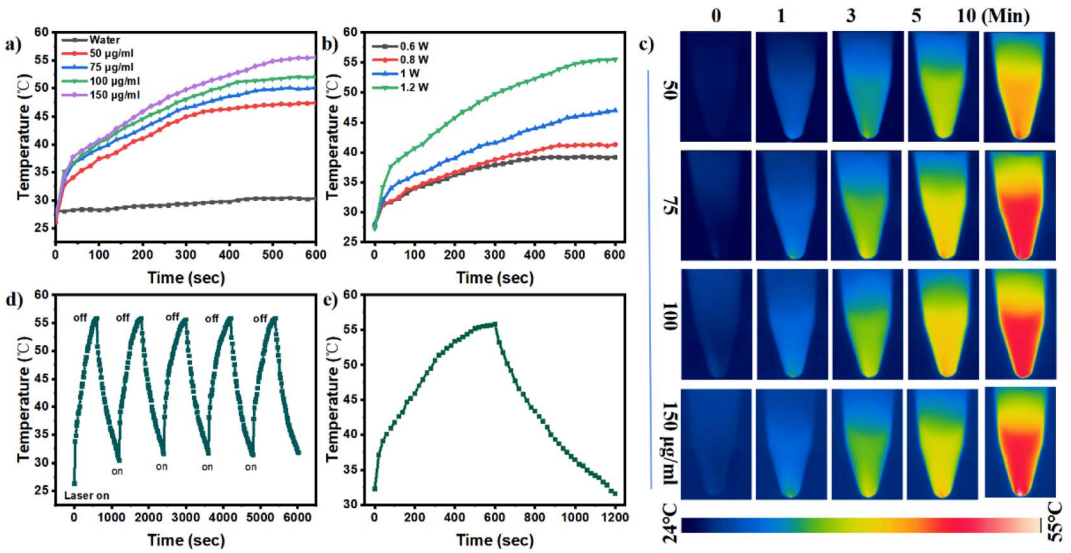

Fig. 3 Photoheating performance of FMC-POP. (a) Photothermal curves of FMC-POP with different concentrations (0, 50, 75, 100 and 150 μg mL^{-1}) in the presence of an 808 nm laser. (b) Photothermal curves of FMC-POP (150 μg mL^{-1}) receiving irradiation under different laser power densities. (c) The infrared thermal photographs of FMC-POP suspension at various concentrations (50, 75, 100 and 150 μg mL^{-1}, respectively) under laser irradiation (1.2 W cm^{-2}). (d) Photothermal stability of FMC-POP under five successive on/off cycles of laser irradiation. (e) The heating and cooling profile of FMC-POP (150 mg mL^{-1}) upon 808 nm laser irradiation for a single on/off cycle.

treatment groups. Meanwhile, TEM was also performed to characterize the membrane integrity of the bacteria and to illuminate the antibacterial effects of different treatment groups by observing the morphological changes in the bacteria.[54] Similar to bacteria treated with PBS (Fig. 5g(I) and h(I)), bacteria treated with FMC-POP (Fig. 5g(II) and h(II)) and

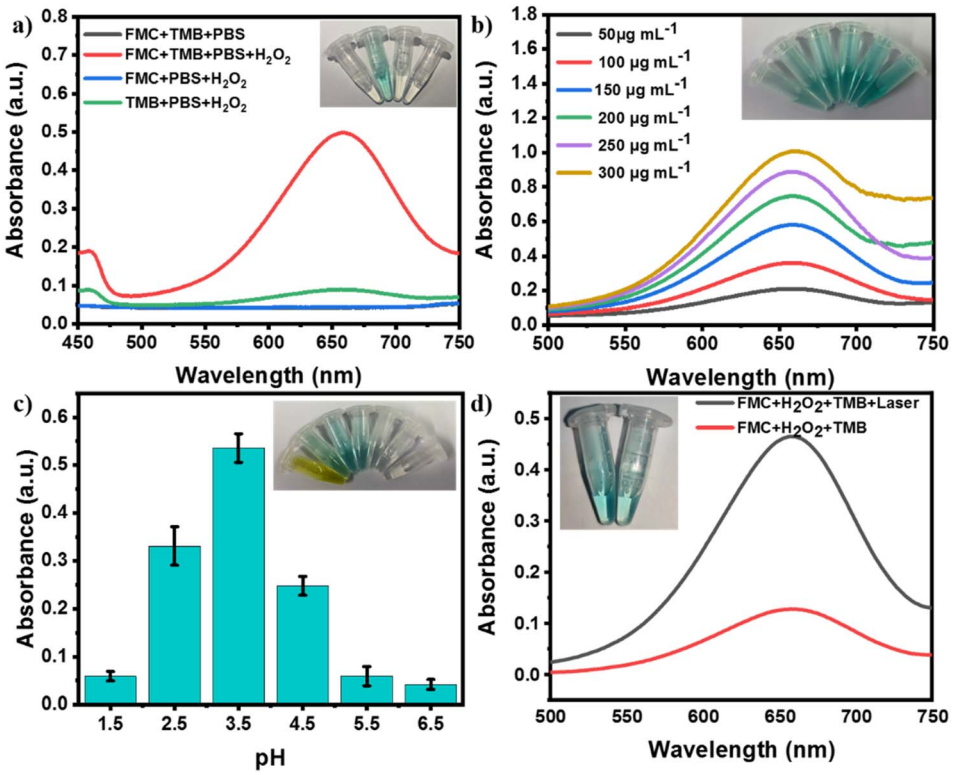

Fig. 4 (a) UV spectra of FMC + TMB + PBS, FMC + TMB + PBS + H_2O_2, FMC + PBS + H_2O_2 and TMB + PBS + H_2O_2. (b) UV spectra of TMB color development curves for different concentrations of FMC. (c) UV spectra of TMB color development reaction systems at different pH conditions at 652 nm. (d) UV spectra of FMC + TMB + PBS + H_2O_2 + laser and FMC + TMB + PBS + H_2O_2. The insets in (a–d) are the corresponding photographs of the reaction systems. FMC refers to FMC-POP.

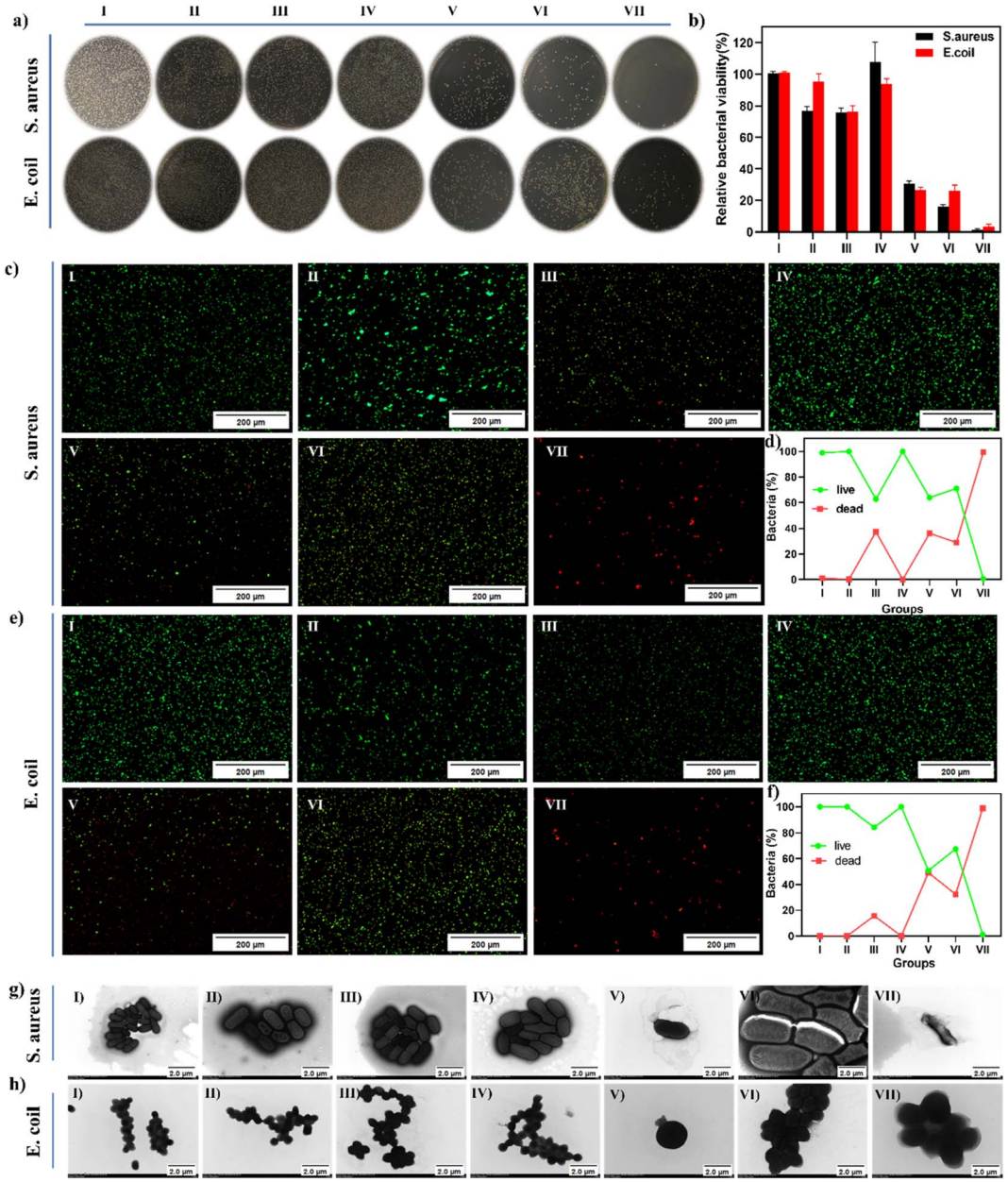

Fig. 5 (a) Photographs of bacterial colonies formed by *S. aureus* and *E. coli* after treatment with (I) PBS, (II) FMC-POP, (III) H_2O_2, (IV) laser, (V) FMC-POP + H_2O_2, (VI) FMC-POP + laser and (VII) FMC-POP + H_2O_2+laser. (b) The bacterial survival rates corresponding to (a) with concentrations of 150 μg mL^{-1} for FMC-POP and 10 mM for H_2O_2. (c) Fluorescence staining images of *S. aureus* after treatment with different groups. (d) Quantification of live–dead staining of various groups of *S. aureus*. (e) Fluorescence staining images of *E. coli* for different treatment groups. (f) Quantification of live–dead staining of various groups of *E. coli*. (g and h) Morphologies of *S. aureus* (g) and *E. coli* (h) after treatment with different groups. Irradiation time: 10 min.

PBS + laser (Fig. 5g(IV) and h(IV)) presented smooth and intact surfaces, indicating the negligible antimicrobial activity of pure FMC-POP. By comparison, the cell membrane of bacteria was wrinkled and became slightly distorted when co-incubated with H_2O_2 (Fig. 5g(III) and h(III)) for 10 min. This result revealed that a low concentration of H_2O_2 alone had only a minor impact on the integrity of the bacterial cell membranes.[55] By contrast, bacteria treated with single-mode PTT or enzymatic therapy, *i.e.*, FMC-POP + H_2O_2 (Fig. 5g(V) and b(V)) and FMC-POP + laser (Fig. 5g(VI) and h(VI)), showed rougher and more wrinkled surfaces. However, when treated with FMC-POP + H_2O_2 + laser, the bacteria exhibited not only significant cellular deformation, but also obvious content leakage, demonstrating the strong synergistic antibacterial ability of PTT and enzymatic therapy for rapid and effective killing of *E. coli* and *S. aureus*.[56]

Conclusions

In summary, a collaborative antibacterial treatment platform based on FMC-POP was successfully constructed for rapid and

effective elimination of bacteria. The low-cost FMC-POP with intrinsic photothermal activity also presented prominent peroxidase-like activity under weak acidic conditions, which could transform the low concentration of H_2O_2 into highly toxic ROS ($^{\bullet}OH$) and thus induce damage to the cell membrane. It is worth noting that further application of NIR irradiation to FMC-POP could not only induce the generation of hyperthermia, but also assist in the conversion of H_2O_2 into $^{\bullet}OH$, thus enhancing the enzymatic therapy, to achieve a satisfactory bactericidal effect at a low dose of antibacterial agent. This antibacterial treatment platform successfully incorporates enzymatic therapy with PTT for combating bacterial infection, which paves the way for the development of new broad-spectrum antibacterial agents.

Conflicts of interest

The authors declare no competing financial interest.

Acknowledgements

This work was supported by the Natural Science Foundation of Shandong Province (ZR2020QB067).

References

1 Q. Jia, Q. Song, P. Li and W. Huang, Rejuvenated Photodynamic Therapy for Bacterial Infections, *Adv. Healthcare Mater.*, 2019, **8**, 1900608.
2 H. Luo, W. Ji, W. Guo, P. Chen, Z. Zhang, X. Xu, B. Yue, W. Tan and B. Zhou, A photoactive Dual-cationic Covalent Organic Framework Encapsulated Sodium Nitroprusside as controllable NO-releasing material for joint cation/photothermal/NO antibacterial therapy, *Microporous Mesoporous Mater.*, 2022, **346**, 112281.
3 J. M. V. Makabenta, A. Nabawy, C. H. Li, S. Schmidt-Malan, R. Patel and V. M. Rotello, Nanomaterial-based therapeutics for antibiotic-resistant bacterial infections, *Nat. Rev. Microbiol.*, 2021, **19**, 23–36.
4 J. Jampilek, Design and discovery of new antibacterial agents: Advances, perspectives, challenges, *Curr. Med. Chem.*, 2018, **25**, 4972–5006.
5 J. Huo, Q. Jia, H. Huang, J. Zhang, P. Li, X. Dong and W. Huang, Emerging photothermal-derived multimodal synergistic therapy in combating bacterial infections, *Chem. Soc. Rev.*, 2021, **50**, 8762–8789.
6 H. Luo, T. Huang, X. Li, J. Wang, T. Lv, W. Tan, F. Gao, J. Zhang and B. Zhou, Synergistic antibacterial and wound-healing applications of an imidazole-based porous organic polymer encapsulated silver nanoparticles composite, *Microporous Mesoporous Mater.*, 2022, **337**, 111925.
7 H. Lou, L. Chu, W. Zhou, J. Dou, X. Teng, W. Tan and B. Zhou, A diselenium-bridged covalent organic framework with pH/GSH/photo-triple-responsiveness for highly controlled drug release toward joint chemo/photothermal/chemodynamic cancer therapy, *J. Mater. Chem. B*, 2022, **10**, 7955–7966.
8 D. Sun, X. Pang, Y. Cheng, J. Ming, S. Xiang, C. Zhang, P. Lv, C. Chu, X. Chen and N. Zheng, Ultrasound-switchable nanozyme augments sonodynamic therapy against multidrug-resistant bacterial infection, *ACS Nano*, 2020, **14**, 2063–2076.
9 H. Lou, H. Fang, T. Wang, D. Wang, Q. Han, W. Zhou, Y. Song, W. Tan and B. Zhou, Biodegradable Porous Polymeric Drug with pH-Stimuli-Responsive Delivery Capacity for Combined Cancer Therapy, *ACS Appl. Polym. Mater.*, 2022, **4**, 714–724.
10 M. Xu, L. Li and Q. Hu, The recent progress in photothermal-triggered bacterial eradication, *Biomater. Sci.*, 2021, **9**, 1995–2008.
11 Y. Tian, Z. Ding, X. Zheng, Y. Li, X. Teng, G. Guo, J. Wang, W. Tan and B. Zhou, Porphyrin-based porous organic polymer coated ZIF-8 nanoparticles as tumor targeted photosensitizer for combination cancer photodynamic/photothermal therapy, *Microporous Mesoporous Mater.*, 2023, **355**, 112562.
12 Y. Su, M. Ding, H. Dong, Y. Hu, D. Yang, J. Shao and B. Huang, Recent advances in nanozymes for combating bacterial infection, *Mater. Chem. Front.*, 2022, **6**, 2596–2609.
13 Y. Zhang, D. Li, J. Tan, Z. Chang, X. Liu, W. Ma and Y. Xu, Near-infrared regulated nanozymatic/photothermal/photodynamic triple-therapy for combating multidrug-resistant bacterial infections via oxygen-vacancy molybdenum trioxide nanodots, *Small*, 2021, **17**, 2005739.
14 B. Halliwell, M. V. Clement and L. H. Long, Hydrogen peroxide in the human body, *FEBS Lett.*, 2000, **486**, 10–13.
15 B. J. Juven and M. D. Pierson, Antibacterial effects of hydrogen peroxide and methods for its detection and quantitation, *J. Food Prot.*, 1996, **59**, 1233–1241.
16 X. Liu, L. Zhao, F. Liu, D. Astruc and H. Gu, Supramolecular redox-responsive ferrocene hydrogels and microgels, *Coord. Chem. Rev.*, 2020, **419**, 213406.
17 J. Yang, L. Yang, Q. Li and L. Zhang, Ferrocene-based multifunctional nanoparticles for combined chemo/chemodynamic/photothermal therapy, *J. Colloid Interface Sci.*, 2022, **626**, 719–728.
18 A. Singh, P. Kumari, A. Raghuvanshi, S. M. Mobin and P. Mathur, Ferrocene-substituted bis (ethynyl) anthracene compounds as anticancer agents, *Appl. Organomet. Chem.*, 2018, **32**, e4071.
19 T. Kanno, K. Nakamura, H. Ikai, K. Kikuchi, K. Sasaki and Y. Niwano, Literature review of the role of hydroxyl radicals in chemically-induced mutagenicity and carcinogenicity for the risk assessment of a disinfection system utilizing photolysis of hydrogen peroxide, *J. Clin. Biochem. Nutr.*, 2012, **51**, 9–14.
20 H. Sun, Q. Zhang, J. Li, S. Peng, X. Wang and R. Cai, Near-infrared photoactivated nanomedicines for photothermal synergistic cancer therapy, *Nano Today*, 2021, **37**, 101073.
21 R. Niu, Y. Liu, Y. Wang and H. Zhang, An Fe-based single-atom nanozyme with multi-enzyme activity for parallel catalytic therapy via a cascade reaction, *Chem. Commun.*, 2022, **58**, 7924–7927.

22 D. Saikat, H. Patrick, B. Teng and Q. Shi, Porous Organic Materials: Strategic Design and Structure–Function Correlation, *Chem. Rev.*, 2017, **117**(3), 1515–1563.
23 A. Slater and A. Cooper, Function-led design of new porous materials, *Science*, 2015, **348**, aaa8075.
24 J. Lee and A. Cooper, Advances in conjugated microporous polymers, *Chem. Rev.*, 2020, **120**, 2171–2214.
25 J. Chakraborty, I. Nath and F. Verpoort, A physicochemical introspection of porous organic polymer photocatalysts for wastewater treatment, *Chem. Soc. Rev.*, 2022, **51**, 1124–1138.
26 Z. Zhang, J. Jia, Y. Zhi, S. Ma and X. Liu, Porous organic polymers for light-driven organic transformations, *Chem. Soc. Rev.*, 2022, **51**, 2444–2490.
27 N. Singh, S. Son, J. An, I. Kim, M. Choi, N. Kong, W. Tao and J. S. Kim, Nanoscale porous organic polymers for drug delivery and advanced cancer theranostics, *Chem. Soc. Rev.*, 2021, **50**, 12883–12896.
28 B. Boro, R. Paul, H. Tan, Q. Trinh, J. Rabeah, C. Chang, C. Pao, W. Liu, N. Nguyen, B. Mai and J. Mondal, Experimental Validation and Computational Predictions Join Forces to Map Catalytic C−H Activation in Ferrocene Metalated Porous Organic Polymers, *ACS Appl. Mater. Interfaces*, 2023, **15**, 21027–21039.
29 R. Paul, C. Sarkar, M. Jain, S. Xu, K. Borah, D. Dao, C. Pao, S. Bhattacharya and J. Mondal, Ferrocene-derived Fe-metalated porous organic polymer for the core planarity-triggered detoxification of chemical warfare agents, *Chem. Commun.*, 2022, **58**, 7789–7792.
30 Z. Xu, L. Hu, J. Ming, X. Cui, M. Zhang, J. Dou, W. Zhang and B. Zhou, Self-gated porous organic polymer as drug delivery system for pH stimuli-responsive controlled Quercetin release, *Microporous Mesoporous Mater.*, 2020, **303**, 110259.
31 S. C. Park, N. H. Kim, W. Yang, J. W. Nah, M. K. Jang and D. Lee, Polymeric micellar nanoplatforms for Fenton reaction as a new class of antibacterial agents, *J. Controlled Release*, 2016, **221**, 37–47.
32 X. Liu, X. Liang, H. Lou, H. Wang, H. Li, S. Zhang, S. Zhu, W. Han and B. Zhou, Ferrocene-based porous organic polymer derived N-doped porous carbon/Fe3C nanocrystal hybrids towards high-efficiency ORR for Zn–air batteries, *Sustainable Energy Fuels*, 2021, **5**, 1067.
33 X. Ding, H. Li, Y. C. Zhao and B. H. Han, Mannitol-based acetal-linked porous organic polymers for selective capture of carbon dioxide over methane, *Polym. Chem.*, 2015, **6**, 5305–5312.
34 B. Guo, S. Wu, Q. Su, W. Liu, P. Ju, G. Li and Q. Wu, New acetal-linked porous organic polymer as an efficient absorbent for CO_2 and iodine uptake, *Mater. Lett.*, 2018, **229**, 240–243.
35 H. Luo, X. Chen, T. Huang, W. Kang, X. Li, Z. Jiang, L. Pang, J. Bai, W. Tan, J. Li and B. Zhou, In situ simultaneously integrating Co-N-C sites and Co9S8 nanoparticles into N,S-doped porous carbon as trifunctional electrocatalysts for Zn–air batteries driving water splitting, *J. Environ. Chem. Eng.*, 2022, **10**, 107203.
36 B. Zhou, F. Yan, X. Li, J. Zhou and W. Zhang, An Interpenetrating Porous Organic Polymer as a Precursor for FeP/Fe_2P-Embedded Porous Carbon toward a pH-Universal ORR Catalyst, *ChemSusChem*, 2019, **12**, 915–923.
37 Q. Song, W. Bian, Q. Yue, B. Zhang, T. Guo, J. Bai, Z. Wang, W. Tan and B. Zhou, Self-etched bimetallic hybrid derived cobalt/zinc dual-sites coordinated N, P-codoped hollow carbon polyhedron for efficient oxygen reduction reaction, *Mater. Today Adv.*, 2023, **17**, 100334.
38 J. Dou, W. Bian, X. Zheng, Q. Yue, Q. Song, S. Deng, L. Wan, W. Tan, W. Li and B. Zhou, A ZIF-based drug delivery system as three-in-one platform for joint cancer therapy, *Mater. Chem. Phys.*, 2023, **297**, 127345.
39 Y. Li, M. Liu and L. Chen, Polyoxometalate built-in conjugated microporous polymers for visible-light heterogeneous photocatalysis, *J. Mater. Chem. A*, 2017, **5**, 13757.
40 W. Guo, X. Luan, P. Sun, T. Wang, H. Luo, X. Li, C. Li, W. Tan, J. Bai, Q. Wang and B. Zhou, A porous carbon layer wrapped Co_3Fe_7 alloy derived from a bimetallic conjugated microporous polymer as a trifunctional electrocatalyst for rechargeable Zn-air batteries and self-powered overall water splitting, *Sustainable Energy Fuels*, 2021, **5**, 6085.
41 A. M. Shultz, O. K. Farha, J. T. Hupp and S. T. Nguyen, Synthesis of catalytically active porous organic polymers from metalloporphyrin building blocks, *Chem. Sci.*, 2011, **2**, 686–689.
42 J. Sun, L. Song, Y. Fan, L. Tian, S. Luan, S. Niu, L. Ren, W. Ming and J. Zhao, Synergistic photodynamic and photothermal antibacterial nanocomposite membrane triggered by single NIR light source, *ACS Appl. Mater. Interfaces*, 2019, **11**, 26581–26589.
43 Q. Wu, R. Peng, Y. Luo, Q. Cui, S. Zhu and L. Li, Antibacterial activity of porous gold nanocomposites via NIR light-triggered photothermal and photodynamic effects, *ACS Appl. Bio Mater.*, 2021, **4**, 5071–5079.
44 W. Yin, J. Yu, F. Lv, L. Yan, L. R. Zheng, Z. Gu and Y. Zhao, Functionalized nano-MoS_2 with peroxidase catalytic and near-infrared photothermal activities for safe and synergetic wound antibacterial applications, *ACS Nano*, 2016, **10**, 11000–11011.
45 M. S. Khan, H. N. Abdelhamid and H. F. Wu, Near infrared (NIR) laser mediated surface activation of graphene oxide nanoflakes for efficient antibacterial, antifungal and wound healing treatment, *Colloids Surf., B*, 2015, **127**, 281–291.
46 J. Li, W. Zhang, W. Ji, J. Wang, N. Wang, W. Wu, Q. Wu, X. Hou and W. Hu, Near infrared photothermal conversion materials: Mechanism, preparation, and photothermal cancer therapy applications, *J. Mater. Chem. B*, 2021, **9**, 7909–7926.
47 Y. Wang, J. Yao, Z. Cao, P. Fu, C. Deng, S. Yan, S. Shi and J. Zheng, Peroxidase-Mimetic Copper-Doped Carbon-Dots for Oxidative Stress-Mediated Broad-Spectrum and Efficient Antibacterial Activity, *Chem. - Eur. J.*, 2022, **28**, e202104174.
48 F. Li, K. Huang, H. Chang, Y. Liang, J. Zhao, S. Yang and F. Liu, A polydopamine coated nanoscale FeS theranostic

platform for the elimination of drug-resistant bacteria via photothermal-enhanced Fenton reaction, *Acta Biomater.*, 2022, **150**, 380–390.

49 W. Yin, J. Yu, F. Lv, L. Yan, L. R. Zheng, Z. Gu and Y. Zhao, Functionalized nano-MoS_2 with peroxidase catalytic and near-infrared photothermal activities for safe and synergetic wound antibacterial applications, *ACS Nano*, 2016, **10**, 11000–11011.

50 K. Yang, L. Hai, Z. Wang, H. Li, W. Yi, Y. Luo, J. Li, L. Deng and D. He, A biofilm microenvironment-responsive one-for-all bactericidal nanoplatform for photothermal-augmented multimodal synergistic therapy of pathogenic bacterial biofilm infection, *J. Mater. Chem. B*, 2022, **10**, 7744–7759.

51 P. Stiefel, S. Schmidt-Emrich, K. Maniura-Weber and Q. Ren, Critical aspects of using bacterial cell viability assays with the fluorophores SYTO9 and propidium iodide, *BMC Microbiol.*, 2015, **15**, 1–9.

52 C. P. Brussaard, D. Marie, R. Thyrhaug and G. Bratbak, Flow cytometric analysis of phytoplankton viability following viral infection, *Aquat. Microb. Ecol.*, 2001, **26**, 157–166.

53 Y. Li, Z. Zhao, J. Zhang, R. T. Kwok, S. Xie, R. Tang and B. Z. Tang, A bifunctional aggregation-induced emission luminogen for monitoring and killing of multidrug-resistant bacteria, *Adv. Funct. Mater.*, 2018, **28**, 1804632.

54 A. H. Phakatkar, E. Firlar, L. Alzate, B. Song, S. Narayanan, R. Rojaee, T. Foroozan, R. Deivanayagam, D. J. Banner, R. Shahbazian-Yassar and T. Shokuhfar, TEM studies on antibacterial mechanisms of black phosphorous nanosheets, *Int. J. Nanomed.*, 2020, **15**, 3071–3085.

55 D. Spuhler, J. A. Rengifo-Herrera and C. Pulgarin, The effect of Fe^{2+}, Fe^{3+}, H_2O_2 and the photo-Fenton reagent at near neutral pH on the solar disinfection (SODIS) at low temperatures of water containing Escherichia coli K12, *Appl. Catal., B*, 2010, **96**, 126–141.

56 Y. Wang, C. Zhang, H. Zhang, L. Feng and L. Liu, A hybrid nano-assembly with synergistically promoting photothermal and catalytic radical activity for antibacterial therapy, *Chin. Chem. Lett.*, 2022, **33**, 4605–4609.